Brain and Whole-Body Imaging in Rhesus Monkeys of ^{11}C-NOP-1A, a Promising PET Radioligand for Nociceptin/Orphanin FQ Peptide Receptors

Yasuyuki Kimura[1,2], Masahiro Fujita[1], Jinsoo Hong[1], Talakad G. Lohith[1], Robert L. Gladding[1], Sami S. Zoghbi[1], Johannes A. Tauscher[3], Nancy Goebl[3], Karen S. Rash[3], Zhaogen Chen[3], Concepcion Pedregal[3], Vanessa N. Barth[3], Victor W. Pike[1], and Robert B. Innis[1]

[1]Molecular Imaging Branch, National Institute of Mental Health, National Institutes of Health, Bethesda, Maryland; [2]Department of Molecular Neuroimaging, Molecular Imaging Center, National Institute of Radiological Sciences, Chiba, Japan; and [3]Eli Lilly and Co., Indianapolis, Indiana

Our laboratory developed (*S*)-3-(2′-fluoro-6′,7′-dihydrospiro [piperidine-4,4′-thieno[3,2-*c*]pyran]-1-yl)-2-(2-fluorobenzyl)-*N*-methylpropanamide (^{11}C-NOP-1A), a new radioligand for the nociceptin/orphanin FQ peptide (NOP) receptor, with high affinity (K_i, 0.15 nM) and appropriate lipophilicity (measured *logD,* 3.4) for PET brain imaging. Here, we assessed the utility of ^{11}C-NOP-1A for quantifying NOP receptors in the monkey brain and estimated the radiation safety profile of this radioligand based on its biodistribution in monkeys. **Methods:** Baseline and blocking PET scans were acquired from head to thigh for 3 rhesus monkeys for approximately 120 min after ^{11}C-NOP-1A injection. These 6 PET scans were used to quantify NOP receptors in the brain and to estimate radiation exposure to organs of the body. In the blocked scans, a selective nonradioactive NOP receptor antagonist (SB-612111; 1 mg/kg intravenously) was administered before ^{11}C-NOP-1A. In all scans, arterial blood was sampled to measure the parent radioligand ^{11}C-NOP-1A. Distribution volume (V_T; a measure of receptor density) was calculated with a compartment model using brain and arterial plasma data. Radiation-absorbed doses were calculated using the MIRD Committee scheme. **Results:** After ^{11}C-NOP-1A injection, peak uptake of radioactivity in the brain had a high concentration (~5 standardized uptake value), occurred early (~12 min), and thereafter washed out quickly. V_T (mL · cm^{-3}) was highest in the neocortex (~20) and lowest in hypothalamus and cerebellum (~13). SB-612111 blocked approximately 50%–70% of uptake and reduced V_T in all brain regions to approximately 7 mL · cm^{-3}. Distribution was well identified within 60 min of injection and stable for the remaining 60 min, consistent with only parent radioligand and not radiometabolites entering the brain. Whole-body scans confirmed that the brain had specific (i.e., displaceable) binding but could not detect specific binding in peripheral organs. The effective dose for humans estimated from the baseline scans in monkeys was 5.0 μSv/MBq. **Conclusion:** ^{11}C-NOP-1A is a useful radioligand for quantifying NOP receptors in the monkey brain, and its radiation dose is similar to that of other ^{11}C-labeled ligands for neuroreceptors. ^{11}C-NOP-1A appears to be a promising candidate for measuring NOP receptors in the human brain.

Key Words: molecular imaging; positron emission tomography; nociceptin/orphanin peptide

J Nucl Med 2011; 52:1638–1645
DOI: 10.2967/jnumed.111.091181

The nociceptin/orphanin FQ peptide (NOP) receptor is a G-protein–coupled receptor, with sequences similar to the classic opioid receptors: μ, δ, and κ (*1*). NOP receptors are involved in a wide range of physiologic responses in the nervous system, cardiovascular system, airways, gastrointestinal tract, urogenital tract, and immune system (*2,3*). In the nervous system, spinal administration of NOP is antinociceptive, but supraspinal administration reverses the effect of exogenous opioids (*4*). Animal studies suggest that the NOP receptor is a viable target for the treatment of variety of diseases such as pain, drug and alcohol abuse, anxiety, depression, and Parkinson disease (*2,5*).

NOP receptor distribution is widespread in the human and nonhuman primate brain. In the postmortem human brain, a ligand specific to the NOP receptor shows high density in the cerebral cortex and striatum and moderate density in the hippocampus and cerebellum (*6*). In the postmortem monkey brain, binding is most abundant in the cerebral cortex, hippocampus, amygdala, striatum, and thalamus and is moderate in the cerebellum (*7*). A PET radioligand for the NOP receptor would allow investigators to determine whether this receptor has an abnormal distribution in various disorders in vivo, including neuropsychiatric ones, and would facilitate the development of drugs that target this binding site. Until recently, no promising radioligand for the NOP receptor had been developed. Ogawa et al. reported 2 radioligands, ^{11}C-methyl-Ro 64-6198 and ^{11}C-CPEB, with high affinity for the NOP receptor, but they have high nonspecific binding to the rat brain in vivo (*8,9*).

Received Mar. 31, 2011; revision accepted Jun. 20, 2011.
For correspondence or reprints contact: Robert B. Innis, Molecular Imaging Branch, National Institute of Mental Health, 10 Center Dr., Bethesda, MD 20892-1026.
E-mail: robert.innis@nih.gov
Published online Aug. 30, 2011.

We recently synthesized a new radioligand—^{11}C-NOP-1A ((*S*)-3-(2′-fluoro-6′,7′-dihydrospiro[piperidine-4,4′-thieno [3,2-*c*]pyran]-1-yl)-2-(2-fluorobenzyl)-*N*-methylpropanamide; Supplemental Fig. 1 [available online only at http://jnm.snmjournals.org])—that has high affinity for the NOP receptor (K_i, 0.15 nM) and appropriate lipophilicity (measured *logD,* 3.4) for PET brain imaging (*10*). We also showed that ^{11}C-NOP-1A had specific (i.e., displaceable) uptake in the monkey brain. The purposes of this study were 2-fold: to assess the utility of ^{11}C-NOP-1A for quantifying NOP receptors in the monkey brain and to estimate the radiation safety profile of this radioligand on the basis of its peripheral biodistribution in monkeys.

MATERIALS AND METHODS

Radioligand Preparation

^{11}C-NOP-1A was labeled by ^{11}C-methylation of an *N*-desmethyl precursor, as described by Pike et al. (*10*). The average specific activity of ^{11}C-NOP-1A at the time of injection was 93 ± 63 GBq/μmol for the 3 baseline scans and 107 ± 66 GBq/μmol for the 3 blocked scans with SB-612111 (*11–14*), a selective nonradioactive NOP receptor antagonist.

Animals

Three male rhesus monkeys (*Macaca mulatta*; mean weight ± SD, 11 ± 0.6 kg) were immobilized with ketamine (10 mg/kg intramuscularly), intubated, and subsequently anesthetized with isoflurane (1%–3% in O_2). Electrocardiograph, body temperature, heart rate, and respiration rate were monitored throughout the experiment. Body temperature was maintained between 36.5°C and 39.0°C. All animal experiments were performed in accordance with the *Guide for the Care and Use of Laboratory Animals* (*15*) and were approved by the National Institute of Mental Health Animal Care and Use Committee.

Measurement of ^{11}C-NOP-1A in Plasma

To determine the stability of ^{11}C-NOP-1A in vitro, approximately 15 kBq of radioligand were incubated with blood and plasma from each monkey for 30 min at room temperature. In blood and plasma, 99.8% ± 0.5% (n = 6) and 99.8% ± 0.5% (n = 6) of radioactivity represented unmetabolized ^{11}C-NOP-1A after incubation, respectively.

A plasma time–activity curve for each scan was created and corrected by the fraction of unmetabolized radioligand. Blood samples (1.0 mL each) were drawn from the femoral artery at 15-s intervals until 120 s, followed by 1-mL samples each at 3, 5, 10, 20, and 30 min; 2-mL samples each were then drawn at 60, 90, and 120 min. Radioactivity in plasma and the in vitro standards were extracted into acetonitrile and analyzed by reversed-phase chromatography with a C_{18} column (Novapak, 4 μm, 100 × 8 mm; Waters Corp.), which was housed in a radial compression module (RCM-100) and eluted at 2 mL/min with methanol:water:triethylamine (80:20:0.1 by volume) as previously described (*16*).

The plasma-free fraction of 2 monkeys was measured by ultrafiltration, as previously described (*17*). The plasma-free fraction, the fraction of the ligand that is not bound to plasma proteins at equilibrium, was 15% ± 2% (n = 4 blood samples).

PET Scans

PET scans at baseline and after NOP-receptor blockade were acquired for each of 3 monkeys. The injected dose of ^{11}C-NOP-1A was 229 ± 13 MBq for the baseline scans and 239 ± 15 MBq for the blocked scans. Dynamic 2-dimensional PET scans were acquired from head to thigh using an Advance tomograph (GE Healthcare). Each monkey was imaged in 4 contiguous 15-cm bed positions in 22 frames per bed position, each of increasing duration (from 30 s to 4 min), for a total scan time of 114 min. Because the brain was acquired in the first of 4 bed positions, the last brain scan was acquired at about 98–102 min after injection. All images were corrected for attenuation and scatter.

For the blocked scans, the selective NOP receptor antagonist SB-612111 (1 mg/kg intravenously, equaling 2.4 μmol/kg), synthesized by Eli Lilly, was injected 10 min before the radioligand. The structure of SB-612111 is shown in Supplemental Figure 1. In all scans, arterial blood was sampled to measure the plasma concentrations of ^{11}C-NOP-1A.

Brain Image Analysis

As an overview, regional time–activity curves were created from volumes of interest that were positioned on the monkey's MR image and then transferred to the coregistered PET image. More specifically, axial MR images of 1.5-mm contiguous slices were obtained using a 1.5-T Signa device (GE Healthcare), with a repetition time of 13.1 ms, echo time of 5.8 ms, and flip angle of 45°. The MR image of each animal was coregistered to the PET image using statistical parametric mapping (version 8 [Wellcome Department of Cognitive Neurology], for Windows [Microsoft]). Both MR and PET images were then spatially normalized to a model monkey brain on the basis of transformation parameters from the MR images. Volumes of interest were drawn on the model monkey brain and applied to the spatially normalized PET images to extract time–activity curves for the following 16 brain regions: prefrontal cortex (7.4 cm^3), basal frontal cortex (0.7 cm^3), parietal cortex (3.2 cm^3), occipital cortex (6.5 cm^3), insula (0.7 cm^3), lateral temporal cortex (4.8 cm^3), medial temporal cortex (1.0 cm^3), amygdala (0.3 cm^3), hippocampus (1.1 cm^3), anterior cingulate cortex (1.6 cm^3), posterior cingulate cortex (0.3 cm^3), caudate (0.9 cm^3), putamen (1.4 cm^3), thalamus (0.8 cm^3), hypothalamus (0.1 cm^3), and cerebellum (5.1 cm^3). All image analyses were conducted using PMOD 3.14 (PMOD Technologies).

Brain Kinetic Analysis

Distribution volume was calculated according to both a 1- and 2-tissue-compartment model and using the serial concentrations of radioactivity in brain and the concentration of parent radioligand in plasma (*18*). Total distribution volume (V_T) was estimated with weighted least squares and the Marquardt optimizer. Brain data for each frame were weighted on the basis of the noise-equivalent counts.

The optimal compartment model (i.e., 1 vs. 2 tissue compartments) was chosen on the basis of the Akaike information criterion (AIC) (*19*), model selection criterion (MSC) (*20*), and F test. The most appropriate model would be the one with the smallest AIC and the largest MSC value. Goodness of fit by 1- and 2-tissue-compartment models was compared with F statistics (*21*). A value of P less than 0.05 was considered significant. The identifiability of V_T was expressed as a percentage and equals the ratio of the SE of V_T divided by the value of V_T itself. A lower percentage indicates better identifiability.

We evaluated the time stability of V_T to determine the minimal scan length necessary for reliable measurements and to indirectly assess whether radiometabolites of ^{11}C-NOP-1A enter brain. We examined the time stability of V_T by increasingly truncating the scan duration from 0–100 min to 0–10 min in 10-min increments.

Dosimetry Analysis

Regions were drawn on source organs that could be identified from 3-dimensional tomographic images: brain, heart, lungs, liver, spleen, gallbladder, kidneys, lumbar vertebrae, small intestine, and urinary bladder. Generously sized regions were used to include all the radioactivity in each organ. The mean recovered activity in PET images above the thigh was 88% of the injected activity. Thus, uptake in each source organ was corrected for this recovery by 88%.

At each time point, the measured activity (i.e., not corrected for decay) of the source organ was expressed as the percentage injected activity. The area under the time–activity curve of each organ was calculated by the trapezoidal method during the 120-min scanning session. The area after the last image to infinity was calculated by assuming that the subsequent decline of radioactivity occurred only via physical decay, without any further biologic clearance. The area under the curve of percentage injected activity from time zero to infinity equals residence time of the organ. To calculate the residence time for the remainder of the body, the residence times for all source organs were summed and subtracted from the fixed theoretic value of $T_{1/2}/\ln 2 = 0.49$ h.

The residence time of all red marrow in the body was estimated from that of lumbar vertebrae. However, a small portion of the radioactivity in lumbar vertebrae may have come from bone but not from red marrow. To conservatively estimate radiation-absorbed doses, we assigned all radioactivity of lumbar vertebrae to red marrow. Applying the reported observation that the mass of red marrow in lumbar vertebrae of *Macaca mulatta* is 17% of the mass of all red marrow in the body (*22*), residence time of red marrow in the entire body was calculated by multiplying that of lumbar vertebrae by 100/17.

The residence times of the monkeys were converted into corresponding human values by multiplying with a factor to scale organ and body weights: $(b_m/o_m) \times (o_h/b_h)$, where b_m and b_h are the body weights of monkey and human, respectively, and o_m and o_h are the organ weights of monkey and human, respectively (Supplemental Table 1).

Radiation-absorbed doses were calculated by entering the residence times for all source organs into OLINDA/EXM 1.0 software (*23*) using the model for a 70-kg adult male.

RESULTS

Pharmacologic Effects

In a total of 6 scans in 3 monkeys, ^{11}C-NOP-1A injection had no significant pharmacologic effects. The injected dose of ^{11}C-NOP-1A was 312 ± 195 pmol/kg for the baseline scans and 283 ± 197 pmol/kg for the blocked scans. In addition, intravenous injection of the NOP receptor antagonist SB-612111 (1 mg/kg, equaling 2.4 μmol/kg) caused no obvious pharmacologic effects. Differences between pre- and postinjection vital signs were less than 15 mm Hg for systemic blood pressure, less than 10/min for pulse, and less than 1°C for body temperature.

Whole-Body Biodistribution and Dosimetry Estimates

Whole-body images were notable for early distribution in the blood pool, accumulation in the target organ (i.e., brain), and excretion of radioactivity via hepatobiliary and urinary routes (Fig. 1; Supplemental Fig. 2). At early time points, radioactivity was prominent in organs with high blood volume, including the kidneys, heart, lung, and liver. The images showed excretion of radioactivity via both hepatobiliary routes (with ~5% injected activity in gallbladder and small intestine at 60 min) and urinary routes (with almost 20% of injected activity in urinary bladder at 120 min). Preinjection of the selective antagonist SB-612111 caused no noticeable change of activity in any organ, except the brain (Fig. 1; Supplemental Fig. 2).

The effective dose, which is a weighted sum of overall exposure to the organs, would be 5.0 μSv/MBq. The organs with the longest residence times were the liver, lungs, and red marrow (Supplemental Table 2). The organs with the highest radiation doses (μGy/MBq) were the gallbladder wall, brain, urinary bladder wall, and liver (Table 1). Because the time–activity curves of all organs, except the brain, were not visibly affected by receptor blockade, we did not do a dosimetry calculation for the 3 blocked scans.

Plasma Analysis

After injection over 1 min, ^{11}C-NOP-1A showed a quick peak and fast washout in plasma (Fig. 2A). In addition, receptor blockade with SB-612111 did not influence the time course or metabolism of the radioligand (Supplemental Fig. 3A). For both baseline and blocked scans, the plasma concentration of ^{11}C-NOP-1A peaked at approximately 2 min and decreased quickly thereafter (Fig. 2A). Receptor blockade did not change the composition of radioactivity in plasma (i.e., percentage of plasma radioactivity that is parent radioligand) or the clearance of ^{11}C-NOP-1A from plasma. The clearance was 407 mL/min at baseline and 434 mL/min after receptor blockade. Finally, the radiometabolites in plasma eluted earlier on reversed-phase high-performance liquid chromatography and are thus all less lipophilic than the parent radioligand ^{11}C-NOP-1A (Supplemental Fig. 3B).

Brain Uptake and Compartmental Analysis

After the injection of ^{11}C-NOP-1A, radioactivity in brain reached high peak levels, washed out quickly, and was appropriately distributed for labeling NOP receptors (Figs. 2B and 3). For example, the brain region with the highest uptake (insula) reached a peak concentration of approximately 6 standardized uptake value at approximately 8 min, and then declined to approximately 30% of peak by the end of the scan at 100 min. For the 16 brain regions, the peak concentration of radioactivity in brain was highest in the insula and amygdala and lowest in hypothalamus and medial temporal cortex. As expected, injection of the NOP receptor antagonist SB-612111 (1 mg/kg intravenously) decreased uptake and increased the rate of washout from all regions.

Receptor binding of ^{11}C-NOP-1A could be quantified in the brain assuming the input of only parent radioligand in arterial plasma. Although total V_T, which is a measure of receptor density, could be reliably quantified with both 1- and 2-tissue-compartment models, we selected the 1-tissue-compartment model for the following reasons. In all baseline

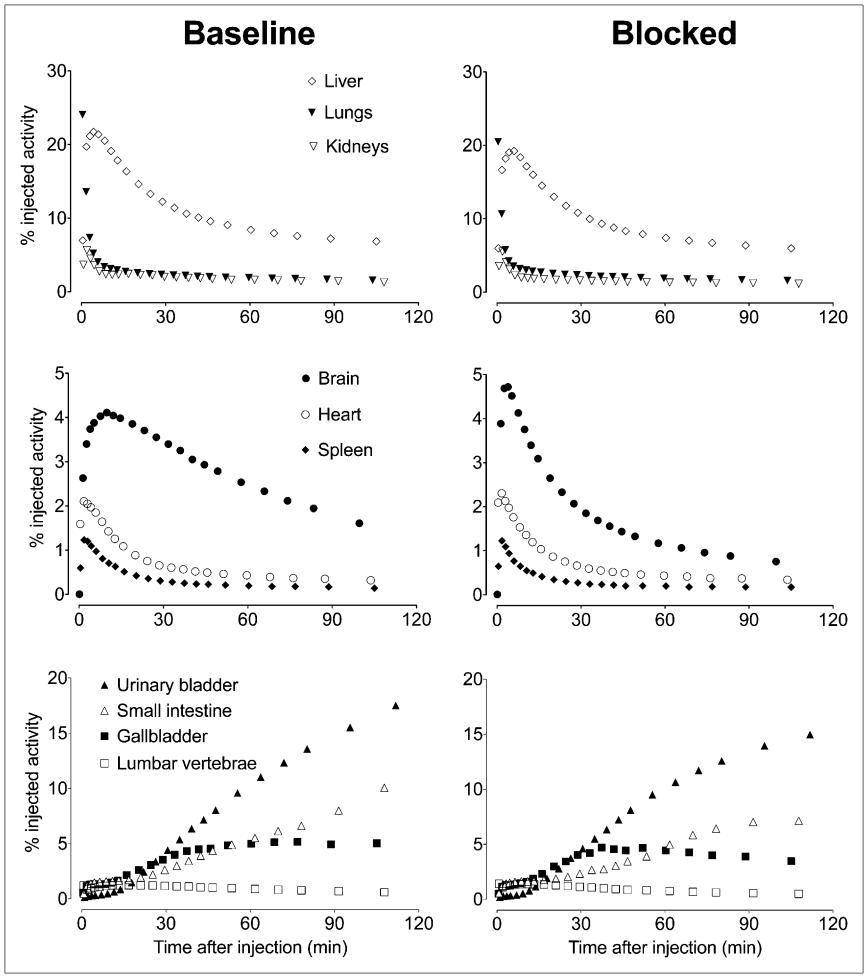

FIGURE 1. Time–activity curves for source organs after ^{11}C-NOP-1A injection at baseline and after receptor blockade with SB-612111. Symbols represent mean from 3 monkeys and are same for each of 3 pairs of panels (baseline and blocked). Data are decay-corrected to time of injection.

experiments, both 1- and 2-tissue-compartment models converged in all regions. However, AIC and MSC values in the 1-tissue-compartment model were, respectively, smaller and larger than those in the 2-tissue-compartment model for all brain regions except for 2 regions in 1 monkey. Nevertheless, differences between 1- and 2-tissue-compartmental fittings were not significant by F tests in any brain region, except for the cerebellum of 1 monkey. Moreover, the 1-tissue-compartment model identified the 2 rate constants (K_1 and k_2) with an SE less than 10% in all regions. In contrast, the 2-tissue compartment model poorly identified the rate constants (K_1, k_2, k_3, and k_4) in some brain regions in all monkeys. Thus, we chose the 1-tissue-compartment model because it adequately described the kinetics of ^{11}C-NOP-1A, and our data lacked adequate information to justify identifying 2 compartments in tissue. Compared with the baseline scans, the blocked scans showed less robust differences between 1- and 2-tissue-compartment models. Largely for the sake of consistency, we applied a 1-tissue-compartment model to both baseline and blocked scans. Independent of whether we used a 1- or 2-tissue-compartment model, the absolute and relative V_T values were unchanged, as was the effect of receptor blockade.

Preinjection of the selective antagonist SB-612111 decreased uptake in all brain regions (Table 2). The decrease in V_T from baseline presumably reflected binding of the radioligand to NOP receptors and will be referred to as specific distribution volume (V_S)—that is, V_T baseline – V_T blocked. Consistent with the distribution of NOP receptors in the monkey brain (*7*), V_S values were highest in the lateral temporal cortex, amygdala, and occipital cortex; lowest in the hypothalamus and cerebellum; and intermediate in other regions. The percentage of specific binding (V_S/V_T) varied from 41% to 67% in the 16 regions examined.

To indirectly assess whether radiometabolites accumulate in brain during the course of the scan, we calculated V_T using increasingly truncated segments of the brain time–activity curves. That is, we examined the time stability of V_T by increasingly truncating the scan duration from 0–100 min to 0–10 min in 10-min increments. For both baseline and blocked scans, the 1-tissue-compartment model successfully identified V_T within 10% of its terminal value (0–100 min) with only the initial 40–60 min of imaging data (Supplemental Fig. 4). Similarly, V_T was well identified (i.e., had low SE values) within 40–60 min of scanning. On the basis of these results, it appears that

TABLE 1
Radiation Dosimetry Estimates for ^{11}C-NOP-1A in Standard Reference Man

Target organ	Radiation dose (μGy/MBq)
Adrenals	3.4
Brain	5.5
Breasts	1.9
Gallbladder wall	35.6
Lower large intestine wall	2.4
Small intestine	4.1
Stomach wall	2.6
Upper large intestine wall	2.8
Heart wall	12.8
Kidneys	13.5
Liver	13.8
Lungs	11.2
Muscle	2.1
Ovaries	2.5
Pancreas	3.5
Red marrow	5.0
Osteogenic cells	4.5
Skin	1.5
Spleen	11.9
Testes	1.8
Thymus	2.3
Thyroid	1.9
Urinary bladder wall	15.7
Uterus	2.8
Total body	2.8
Effective dose (μSv/MBq)	5.0

^{11}C-NOP-1A binding to receptors in the brain can be quantified from about 1 h of imaging data combined with serial concentration of the parent radioligand in arterial plasma. Notably, V_T values were stable for the last half hour of imaging (60–100 min), which is consistent with (but does not prove) a lack of accumulation of radiometabolites in the brain. Consistent with this interpretation, radiometabolites of ^{11}C-NOP-1A in plasma were less lipophilic than the parent radioligand (Supplemental Fig. 3B).

V_T was also calculated using the graphical approach of Logan (*24*), which does not specify a particular compartmental configuration. The slope of the linear portion of the Logan plot, which equals V_T, was well identified (Supplemental Fig. 5).

DISCUSSION

This study used an efficient experimental design in monkeys to acquire both brain and whole-body images after each injection of ^{11}C-NOP-1A to quantify NOP receptors in the brain and to estimate radiation exposure for future studies in humans. We found that brain uptake was well and stably quantified as total V_T, which equals the ratio at equilibrium of the concentration of radioligand in brain to that in plasma. V_T was well identified (i.e., low SE) and stably determined after about 60 min of brain imaging and concurrent measurements of arterial input function (i.e., the concentrations over time of ^{11}C-NOP-1A, separated from radiometabolites). The selective antagonist SB-612111 decreased V_T by approximately 40%–70% in 16 regions of brain, suggesting that most brain uptake was specifically bound to NOP receptors. Whole-body scans confirmed that the brain has specific (i.e., displaceable) binding but could not detect specific binding in peripheral organs. In assessing radiation exposure to the entire body, the effective dose for humans estimated from the baseline scans in monkeys was 5.0 μSv/MBq, which is similar to that of many other ^{11}C-labeled radioligands used for brain imaging (*25*).

Brain Distribution and Kinetics

After ^{11}C-NOP-1A injection, the brain radioactivity peaked relatively early (~8 min) and washed out quickly thereafter (e.g., radioactivity in insula declined to approximately 30% of peak at the end of the 2-h scan). Both these characteristics suggested that brain uptake could be quantified as receptor binding using compartmental modeling, because the entire dataset would reflect the kinetics of both association and dissociation binding to the target. In fact, we found that uptake was well identified (i.e., had low SE) using both a 1-tissue-compartment model and Logan graphical analysis. One-tissue-compartment fitting does not mean that all radioactivity in the brain was bound to NOP receptors. In fact, the blocked studies demonstrated uniform nonspecific binding of about 7 mL · cm^{-3}. Instead, the superior fitting with 1 tissue compartment implies that the brain data had enough noise that the model could not distinguish with adequate statistical confidence the kinetics of specific and nonspecific binding of the radioligand. Although we could not reliably distinguish 2 separate kinetic phenomena in brain, the combination of both was well identified as V_T, which is the sum of specific (V_S) and nondisplaceable (V_{ND}) uptake (*18*). In addition, we could calculate V_T with Logan graphical analysis, which does not assume a specific number of compartments (Supplemental Fig. 1). V_T was stably identified within the first hour of the 2-h scanning session. That is, the identification of the same value of V_T for the last hour of the scan showed that the parent radioligand could completely account for radioactivity in brain. This result is consistent with, but does not prove, that radiometabolites do not accumulate in brain. As a counterexample, we previously found that V_T in the rat brain was stably identified despite the presence of radiometabolites (*26*). In that case, stability was possible because radiometabolites remained a constant percentage of total radioactivity in brain.

One disadvantage to using V_T as the outcome measure in human studies is that we were primarily interested in only the specific (or receptor-bound) component of brain uptake. Nevertheless, the percentage of specific binding of ^{11}C-NOP-1A in the monkey brain was relatively high; if humans have a similar percentage of specific binding, V_T will reasonably reflect receptor availability. In addition, our blocked studies showed that the dose of the antagonist strongly affected specific binding in all regions of brain. That is, after a single dose of SB-612111 (1 mg/kg intra-

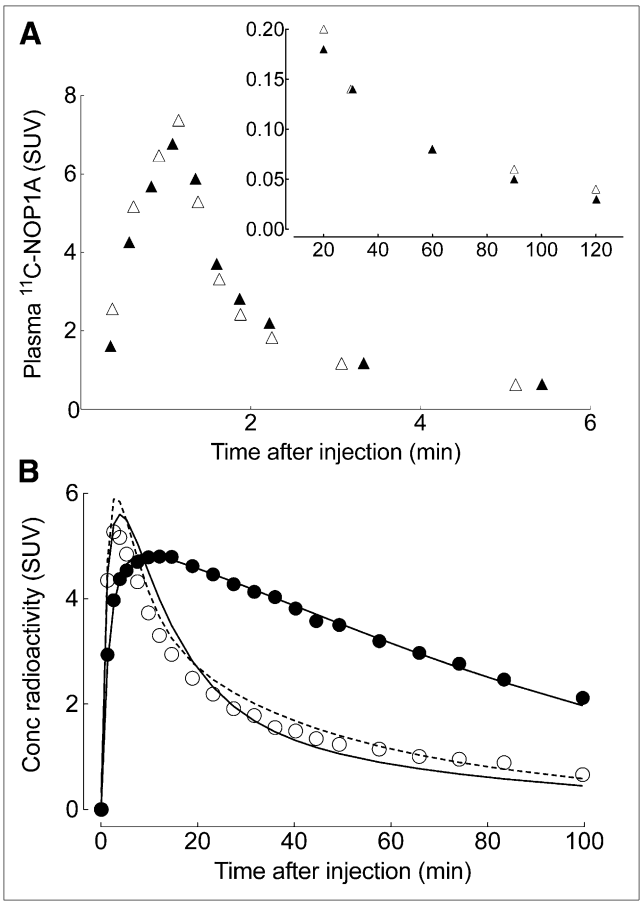

FIGURE 2. Representative time–activity curves of ^{11}C-NOP-1A in plasma and brain at baseline and after receptor blockade with SB-612111 in single monkey. (A) ^{11}C-NOP-1A concentration, separated from radiometabolites, in arterial plasma is plotted at baseline (▲) and after receptor blockade (△). Values from 0 to 6 min and from 20 to 100 min are plotted on separate graphs, which differ in range of *y*-axis. (B) Concentrations of radioactivity in occipital cortex after injection of ^{11}C-NOP-1A are shown at baseline (●) and after receptor blockade (○). Measured brain data were fit with 1-tissue (solid line) and 2-tissue (dotted line)-compartment models. At baseline conditions, 2 fittings overlap almost completely.

venously), radioactivity in all regions was reduced to a single value of V_T (~7 mL · cm^{-3}), showing that no regionally selective specific binding remained. The fact that all regions of monkey brain showed specific binding suggests, but does not prove, that human studies will not be able to use a reference tissue model, which would avoid the arterial catheter. The rhesus brain is about 10 times smaller than the human brain, and partial-volume errors cause spill-in of radioactivity from adjacent areas. The larger human brain may have regions with no (or limited) displaceable uptake that could hypothetically be used as a reference region.

Peripheral Distribution

Although NOP receptors exist in a wide variety of peripheral organs such as heart, pancreas, and spleen (*27*), we could not identify any organ other than the brain that had displaceable binding in monkeys. The lack of displaceable binding in peripheral organs may have been caused by a low density of receptors, the presence of confounding radiometabolites, or the presence of high activity in adjacent regions that spilled into the target organs. These conditions may not apply in humans. In fact, ongoing whole-body scans with ^{11}C-NOP-1A in healthy human subjects show distinct uptake in the heart, pancreas, and spleen (T.G. Lohith, unpublished data, 2011). Similar to our current studies in monkeys, receptor blockade would be necessary in humans to confirm that this peripheral uptake reflects NOP receptor binding.

Dosimetry

The effective dose of ^{11}C-NOP-1A (5.0 μSv/MBq) was similar to that of many other ^{11}C-labeled radioligands and suggests that it can be used in humans at similar safety levels. We recently gathered the dosimetry results from human whole-body imaging of thirty-seven ^{11}C-labeled radioligands and found that the effective dose was 5.5 ± 2.0 μSv/MBq (mean ± SD), with a range of 3.0–16.0 μSv/MBq (C. Hines et al., unpublished data, 2011). However, the present estimate of the effective dose in humans of ^{11}C-NOP-1A may be biased for 3 reasons. First, the estimate was based on scaling factors (Supplemental Table 1) to partially correct for the varying size of organs in monkey versus man. Second, the dose to red marrow sampled only the lumbar vertebrae and then extrapolated to the entire mass of marrow in the body. Third, our results were based on only 3 monkeys. Biodistribution studies in humans will thus be necessary to confirm or refute these estimates.

CONCLUSION

Our results demonstrated that ^{11}C-NOP-1A reliably quantified NOP receptors in the monkey brain, that its specific binding represented 50%–70% of total uptake in various brain regions, and that its radiation dose was similar to that of other ^{11}C-labeled ligands for neuroreceptors. Thus,

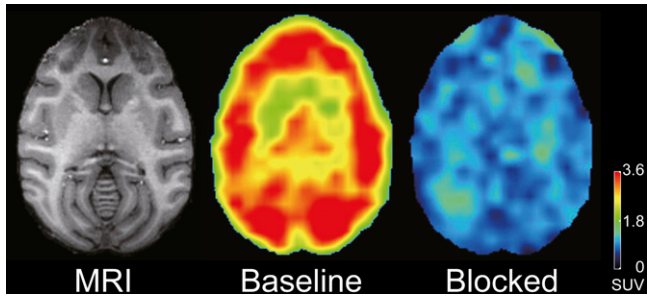

FIGURE 3. Transaxial PET images of brain uptake at baseline and after receptor blockade in same monkey. PET images from 40 to 80 min after injection of ^{11}C-NOP-1A were summed, and pixel values represent mean concentration of radioactivity (standardized uptake value). Monkey was injected with 222 MBq of ^{11}C-NOP-1A at baseline and 222 MBq after receptor blockade. Radioactivity concentration was expressed as standardized uptake value (SUV), which normalizes for injected activity and body mass. Coregistered MR image shows that PET slice extends through caudate, putamen, and cerebellum.

TABLE 2
Distribution Volume of ^{11}C-NOP-1A in Monkey Brain

Organ	V_T (mL · cm^{-3})				V_S (mL · cm^{-3}), baseline − blocked	V_S/V_T (%)
	Baseline		Blocked			
	Mean	SD	Mean	SD		
Prefrontal cortex	18.1	0.9	6.6	2.3	11.6	64
Basal frontal cortex	16.6	1.0	6.1	1.7	10.5	63
Parietal cortex	19.3	2.5	6.8	2.2	12.5	65
Occipital cortex	20.4	2.2	6.6	1.8	13.7	67
Insula	19.8	2.2	7.5	1.9	12.3	62
Lateral temporal cortex	21.3	1.0	7.2	2.0	14.2	66
Medial temporal cortex	16.5	1.3	6.6	1.2	9.9	60
Amygdala	21.0	3.7	7.3	1.8	13.7	65
Hippocampus	18.1	3.0	7.1	1.5	11.0	61
Anterior cingulate	17.7	1.4	7.4	1.8	10.3	58
Posterior cingulate	17.6	1.4	7.2	1.8	10.4	59
Caudate	15.3	0.2	7.2	1.9	8.1	53
Putamen	16.0	1.3	7.6	1.9	8.5	53
Thalamus	16.2	0.7	8.0	2.0	8.2	51
Hypothalamus	12.6	1.2	7.4	1.8	5.2	41
Cerebellum	12.9	1.1	6.7	1.4	6.2	48

^{11}C-NOP-1A is a promising candidate for measuring NOP receptors in human brain.

DISCLOSURE STATEMENT

The costs of publication of this article were defrayed in part by the payment of page charges. Therefore, and solely to indicate this fact, this article is hereby marked "advertisement" in accordance with 18 USC section 1734.

ACKNOWLEDGMENTS

We thank Kacey Anderson, Leah P. Dickstein, Kimberly Jenko, Nobuyo Kimura, Cheryl L. Wallisch, Jeih-San Liow, Harushige Ozaki, and the staff of the PET Department for assistance in completing these studies and PMOD Technologies (Zurich, Switzerland) for providing its image analysis and modeling software. Ioline Henter provided invaluable editorial assistance. Garth Terry created the table for scaling factors for organs in monkey and man. This study was supported by the Intramural Research Program of the National Institute of Mental Health, National Institutes of Health, and by a Cooperative Research and Development Agreement with Eli Lilly. No other potential conflict of interest relevant to this article was reported.

REFERENCES

1. Mollereau C, Parmentier M, Mailleux P, et al. ORL1, a novel member of the opioid receptor family: cloning, functional expression and localization. *FEBS Lett.* 1994;341:33–38.
2. Chiou L-C, Liao Y-Y, Fan P-C, et al. Nociceptin/orphanin FQ peptide receptors: pharmacology and clinical implications. *Curr Drug Targets.* 2007;8:117–135.
3. Mogil JS, Grisel JE, Reinscheid RK, Civelli O, Belknap JK, Grandy DK. Orphanin FQ is a functional anti-opioid peptide. *Neuroscience.* 1996;75:333–337.
4. Grisel JE, Mogil JS, Belknap JK, Grandy DK. Orphanin FQ acts as a supraspinal, but not a spinal, anti-opioid peptide. *Neuroreport.* 1996;7:2125–2129.
5. Lambert DG. The nociceptin/orphanin FQ receptor: a target with broad therapeutic potential. *Nat Rev Drug Discov.* 2008;7:694–710.
6. Berthele A, Platzer S, Dworzak D, et al. [^{3}H]-nociceptin ligand-binding and nociceptin opioid receptor mRNA expression in the human brain. *Neuroscience.* 2003;121:629–640.
7. Bridge KE, Wainwright A, Reilly K, Oliver KR. Autoradiographic localization of ^{125}I[Tyr^{14}] nociceptin/orphanin FQ binding sites in macaque primate CNS. *Neuroscience.* 2003;118:513–523.
8. Ogawa M, Hatano K, Kawasumi Y, et al. Synthesis and evaluation of 1-[(3*R*,4*R*)-1-cyclooctylmethyl-3-hydroxymethyl-4-piperidyl]-3-[^{11}C]ethyl-1,3-dihydro-2*H*-benzimidazol-2-one as a brain ORL1 receptor imaging agent for positron emission tomography. *Nucl Med Biol.* 2003;30:51–59.
9. Ogawa M, Hatano K, Kawasumi Y, Wichmann J, Ito K. Synthesis and in vivo evaluation of [^{11}C]methyl-Ro 64-6198 as an ORL1 receptor imaging agent. *Nucl Med Biol.* 2001;28:941–947.
10. Pike VW, Rash KS, Chen Z, et al. Synthesis and evaluation of radioligands for imaging brain nociceptin/orphanin FQ peptide (NOP) receptors with positron emission tomography. *J Med Chem.* 2011;54:2687–2700.
11. Zaratin PF, Petrone G, Sbacchi M, et al. Modification of nociception and morphine tolerance by the selective opiate receptor-like orphan receptor antagonist (-)-*cis*-1-methyl-7-[[4-(2,6-dichlorophenyl)piperidin-1-yl]methyl]-6,7,8,9-tetrahydro-5*H*-benzocyclohepten-5-ol (SB-612111). *J Pharmacol Exp Ther.* 2004;308:454–461.
12. Rizzi A, Gavioli EC, Marzola G, et al. Pharmacological characterization of the nociceptin/orphanin FQ receptor antagonist SB-612111 [(-)-*cis*-1-methyl-7-[[4-(2,6-dichlorophenyl)piperidin-1-yl]methyl]-6,7,8,9-tetrahydro-5*H*-benzocyclohepten-5-ol]: in vivo studies. *J Pharmacol Exp Ther.* 2007;321:968–974.
13. Spagnolo B, Carrà G, Fantin M, et al. Pharmacological characterization of the nociceptin/orphanin FQ receptor antagonist SB-612111 [(-)-*cis*-1-methyl-7-[[4-(2,6-dichlorophenyl)piperidin-1-yl]methyl]-6,7,8,9-tetrahydro-5*H*-benzocyclohepten-5-ol]: in vitro studies. *J Pharmacol Exp Ther.* 2007;321:961–967.
14. Liao Y, Jiang F, Chiou L. Quantitative study of the antagonistic effect of (-)-*cis*-1-Methyl-7-[[4-(2,6-dichlorophenyl)piperidin-1-yl]methyl]-6,7,8,9-tetrahydro-5*H*-benzocyclohepten-5-ol (SB-612111) on nociceptin/orphanin FQ-mediated potassium channel activation in rat periaqueductal gray slices. *Eur J Pharmacol.* 2011;657:84–88.
15. *Guide for the Care and Use of Laboratory Animals.* Washington, DC: National Academy Press; 1996.
16. Zoghbi SS, Shetty HU, Ichise M, et al. PET imaging of the dopamine transporter with ^{18}F-FECNT: a polar radiometabolite confounds brain radioligand measurements. *J Nucl Med.* 2006;47:520–527.
17. Gandelman MS, Baldwin RM, Zoghbi SS, Zea-Ponce Y, Innis RB. Evaluation of ultrafiltration for the free-fraction determination of single photon emission computed tomography (SPECT) radiotracers: β-CIT, IBF, and iomazenil. *J Pharm Sci.* 1994;83:1014–1019.
18. Innis RB, Cunningham VJ, Delforge J, et al. Consensus nomenclature for *in vivo* imaging of reversibly binding radioligands. *J Cereb Blood Flow Metab.* 2007;27:1533–1539.
19. Akaike H. A new look at the statistical model identification. *IEEE Trans Auto Cont.* 1974;19:716–723.

20. Fujita M, Seibyl JP, Verhoeff NP, et al. Kinetic and equilibrium analyses of [^{123}I] epidepride binding to striatal and extrastriatal dopamine D_2 receptors. *Synapse.* 1999;34:290–304.
21. Hawkins RA, Phelps ME, Huang SC. Effects of temporal sampling, glucose metabolic rates, and disruptions of the blood-brain barrier on the FDG model with and without a vascular compartment: studies in human brain tumors with PET. *J Cereb Blood Flow Metab.* 1986;6:170–183.
22. Taketa ST, Carsten AL, Cohn SH, Atkins HL, Bond VP. Active bone marrow distribution in the monkey. *Life Sci.* 1970;9:169–174.
23. Stabin MG, Sparks RB, Crowe E. OLINDA/EXM: the second-generation personal computer software for internal dose assessment in nuclear medicine. *J Nucl Med.* 2005;46:1023–1027.
24. Logan J, Fowler JS, Volkow ND, et al. Graphical analysis of reversible radioligand binding from time-activity measurements applied to [*N*- ^{11}C-methyl]-(-)-cocaine PET studies in human subjects. *J Cereb Blood Flow Metab.* 1990;10:740–747.
25. Cropley V, Fujita M, Musachio J, et al. Whole-body biodistribution and estimation of radiation-absorbed doses of the dopamine D_1 receptor radioligand ^{11}C-NNC 112 in humans. *J Nucl Med.* 2006;47:100–104.
26. Terry G, Liow J-S, Chernet E, et al. Positron emission tomography imaging using an inverse agonist radioligand to assess cannabinoid CB_1 receptors in rodents. *Neuroimage.* 2008;41:690–698.
27. Dumont M, Lemaire S. Characterization of the high affinity [^{3}H]nociceptin binding site in membrane preparations of rat heart: correlations with the non-opioid dynorphin binding site. *J Mol Cell Cardiol.* 1998;30:2751–2760.